Int. J. Electrochem. Sci., 15 **(2020)** 1347 – 1362, doi: 10.20964/2020.02.06

International Journal of
ELECTROCHEMICAL
SCIENCE
www.electrochemsci.org

Electrochemical Sensor Based on Three-Dimensional Nitrogen-Doped Nanostructured Porous Carbon from Edible *Ulva lactuca* L with a Potentially Wide Application

Jianhua Qin[1], *Ying Zuo*[2], *Haiyu Yu*[1], *Jinzhi Yu*[1], *Xinyue Chen*[1], *Junling Zhang*[1], *Jubo Lv*[1,*], *Hui Xu*[1,*], *Shanmin Gao*[1], *Faju Hou*[1] *and Linlin Zhong*[1]

[1] School of Chemistry and Materials Science, Ludong University, Yantai 264025, P. R. China
[2] Department of Gynecology, The Affiliated Yantai Yuhuangding Hospital of Qingdao University, Yantai, 264000, China
[*]E-mail: Jubolv@163.com (J. Lv); xuhui235@163.com (H. Xu)
Jianhua Qin and Ying Zuo contributed equally to this work.

Received: 22 September 2019 / *Accepted:* 21 November 2019 / *Published:* 30 December 2019

A simple method consisting of a one-step carbonization under a N_2 atmosphere without an activation agent is used for preparing three-dimensional nitrogen-doped nanostructured porous carbons (3D-NNPCs) from edible *Ulva lactuca* L. It has been proposed for environmentally friendly and inexpensive electrochemical sensing.. The prepared 3D-NNPCs have a high specific surface area of 1683.54 $m^2 g^{-1}$, a large pore volume of 1.09 $cm^3 g^{-1}$, a hierarchical porous structure and a high density of defective sites, all of which are beneficial for electrocatalysis. Using a 3D-NNPC-modified glassy carbon electrode (3D-NNPC/GCE), ascorbic acid (AA) is first chosen as a model to study the electrocatalytic performance. The electrode exhibits a greatly decreased overpotential (-0.015 V vs. Ag/AgCl), a lower limit of detection with a sensitivity of 0.055 $\mu A \cdot \mu M^{-1} \cdot cm^{-2}$, a wide linear range spanning 4 orders of magnitude (1 μM-10 mM), and a good selectivity. The above results show that the electrode has promise for practical application in food analysis. In addition, its potentially wide application is examined by using voltammetric determination for other biomolecules.

Keywords: Electrochemical sensor; potentially wide application; food analysis; three-dimensional nitrogen-doped nanostructured porous carbons; edible *Ulva lactuca* L.

1. INTRODUCTION

Carbon nanomaterials such as graphene [1-4], carbon nanotubes (CNTs) [3-6], and porous carbon [7, 8] have been widely applied for electrochemical analysis owing to their inert chemical properties, wide potential windows and high electrocatalysis performance for a wide range of analytes. Although graphene is a great candidate in various electrochemical applications, its preparation from

graphite is complicated, and it is easy to cause an explosion in the process of oxidising graphite. Similarly, the preparation of CNTs requires a complex instrumental setup. Porous carbon is a potential promising material. Metal-organic frameworks (MOFs) [9-11], polymer spheres [12, 13], polybenzoxazine-based polymer [14] and hypercrosslinked polymers [15] are typical precursors to prepare porous carbon, which requires tedious templating or activation procedures. Biomass-based porous carbon, utilizing naturally abundant and renewable resources [16-18], has triggered immense interest in recent years due to its low cost, nontoxicity and good chemical stability.

Ulva lactuca L., a kind of abundant biomass from the sea, is an edible green alga in the family Ulvaceae, which has been widely used as a vegetable for soups and salads, a drug for blood pressure reduction or as biosorbents [19] to remove heavy metals from contaminated waters. However, the rampant growth of algae can lead to marine pollution [20-22]. *Ulva lactuca* L. contains various organic compounds and soluble salt, enabling it to be a good precursor of carbon materials. Until now, all kinds of algae have been reported for the preparation of porous carbon materials for various applications, e.g., supercapacitor [23-26], catalyst support [27], CO_2 capture [25], and adsorbents [28]. However, to obtain high specific surface area and large pore volume, most of them need an addition of activation agents such as KOH [23, 26] or NaOH [7, 29], which is complex and not environmentally friendly. In this manuscript, a three-dimensional nitrogen-doped nanostructured porous carbon (3D-NNPC) from edible *Ulva lactuca* L. is synthesized via a one-step carbonization under a N_2 atmosphere without an activation agent. The prepared porous carbon incorporates multiple types of pores and has a high specific surface area, large pore volume and high density of defective sites, which is beneficial for voltammetric determination of all kinds of small biomolecules. Using ascorbic acid (AA) as a model, a 3D-NNPC-modified glass carbon electrode (3D-NNPC/GCE) exhibits an extremely wide linear range, good selectivity, and low detection limit. Therefore, it has potential for practical application in food analysis.

2. EXPERIMENTAL SECTION

2.1. Reagents

Fresh *Ulva lactuca* L. (Figure S1 in Supporting Information) was obtained from the coastal zone of Yantai, Shandong Province. Multi-walled carbon nanotubes (MWCNTs) were supplied from Shenzhen Nanotech Port Ltd., China (purity>95%). D-(+)-glucose (GLU) anhydrous and *N,N'*-dimethylformamide (DMF) were obtained from Sinopharm Chemical Reagent Co., Ltd. L-ascorbic acid (AA, >99.7%) was obtained from Tianjin Ruijin Special Chemicals Reagent Co., Ltd. Dopamine hydrochloride (DA-HCl) was purchased from Sigma-Aldrich. Uric acid (UA) and tyrosine (Tyr) were supplied from Alfa Aesar. L-glutathione (GSH) was obtained from Chengdu Aikeda Chemical Reagent Co., Ltd. L-cysteine (L-Cys) was purchased from Tianjin Fuchen Chemicals Reagent Co., Ltd.

All other chemicals were of analytical grade and used directly without further purification. All solutions were prepared with ultrapure water (conductivity was 18.25 MΩ·cm). Milk, beer, kiwi fruit, tomato and honey were obtained from a local supermarket in Yantai.

2.2. Instrumentation

JEM-1230 transmission electron microscopy (TEM) was used to obtain the morphologies of the prepared 3D-NNPCs. Scanning electron microscopy (SEM) images were obtained by using a SU8010 (Hitachi). Power X-ray diffraction (XRD) results were performed by scanning from 5° to 80° on a Rigaku SmartLab III diffractometer using Cu Kα radiation (λ=1.5406 Å). The Raman spectra were recorded using a Horiba spectrometer (LabRAM HR Evolution, Japan) set to an excitation wavelength of 532 nm. An ASAP2020 instrument was used to measure N_2 adsorption-desorption isotherms. X-ray photoelectron spectroscopy (XPS) was recorded on an ESCALAB Xi^+ photoelectron spectrometer made by Thermo Fisher Scientific, USA. Fourier transform infrared (FT-IR) spectroscopy of 3D-NNPCs was recorded in the range of 400 to 4000 cm^{-1} on a Nicolet MAGNA-IR 550 (Series II) spectrophotometer.

2.3. Preparation of 3D-NNPCs

3D-NNPCs were synthesized by using a simple one-step carbonization under a N_2 atmosphere without an activation agent. Typically, fresh *Ulva lactuca* L. from the ocean was thoroughly washed with ultrapure water, cut into pieces and dried at 80 °C for four hours. After being fully ground in an agate mortar, the resulting material was carbonized at 800 °C (3 °C min^{-1}) under a nitrogen (N_2) atmosphere for 3 h. To remove soluble impurities, the obtained black solid was treated with 6 M HCl and 6 M KOH for 12 h at 60 °C. After drying at 70 °C for 10 h and further grinding, 3D-NNPCs were obtained.

2.4. Electrode preparation and modification

Before the experiment, a GCE was polished with 1, 0.3 and 0.05 μm alumina powder to a mirror finish. Then, the obtained bare GCE was ultrasonically cleaned in ethanol and ultrapure water for a few minutes before being dried under a N_2 gas flow. Three microlitres of 3D-NNPC suspension (in DMF, 2 mg mL^{-1}) was drop-cast on the surface of the precleaned GCE. After drying at 60 °C, the drop-casting and drying steps were repeated three times to obtain 3D-NNPC/GCE.

2.5. Electrochemical determination

All electrochemical experiments, including cyclic voltammetry (CV), differential pulse voltammetry (DPV) and electrochemical impedance spectroscopy (EIS), were carried out on a CHI 660C electrochemical workstation (CH Instrument, Shanghai, China) with a conventional three-electrode system. An Ag/AgCl (3 M KCl) electrode was used as the reference electrode, and a Pt wire was used as the auxiliary electrode. A modified GCE (3 mm in diameter, with a geometric area of 0.07 cm^2) was used as the working electrode. CV was conducted from -0.40 to 0.60 V for the voltammetric behaviour of AA in 0.1 M phosphate buffer containing 0.1 M NaCl (pH 7.5). After optimizing the pH for the method, DPV was adopted for quantitative analysis of AA in 0.1 M phosphate buffer containing 0.1 M

NaCl (pH 7.5). EIS was performed on the different electrodes in 10 mM $[Fe(CN)_6]^{4-/3-}$ containing 0.1 M KCl in a frequency range of 0.01 Hz to 100 kHz with an amplitude of 5 mV. For real sample analysis, different known amounts of AA standard solution (10000, 100, 10 μM) were added to diluted real food or beverages, such as milk (2%), beer (2%), homemade kiwi juice (2%), homemade tomato juice (2%), and honey (0.2%). Recovery was calculated according to the obtained peak current.

3. RESULTS AND DISCUSSION

3.1. Characterization of 3D-NNPCs

Figure 1 shows representative SEM and TEM images of the as-synthesized 3D-NNPCs. The surface morphology and microstructure can be demonstrated by SEM (Figure 1A). The 3D-NNPCs exhibit a three-dimensional (3D) porous structure with different sizes. The pore structure can be clearly seen from the TEM images. The TEM image in Figure 1B reveals that there are mainly microporous and mesoporous structures of different sizes on 3D-NNPCs. The micropores and mesopores cover the whole surface of the 3D-NNPCs, enhancing the specific surface area and the pore volume. A well-formed 3D network can accelerate electron conduction.

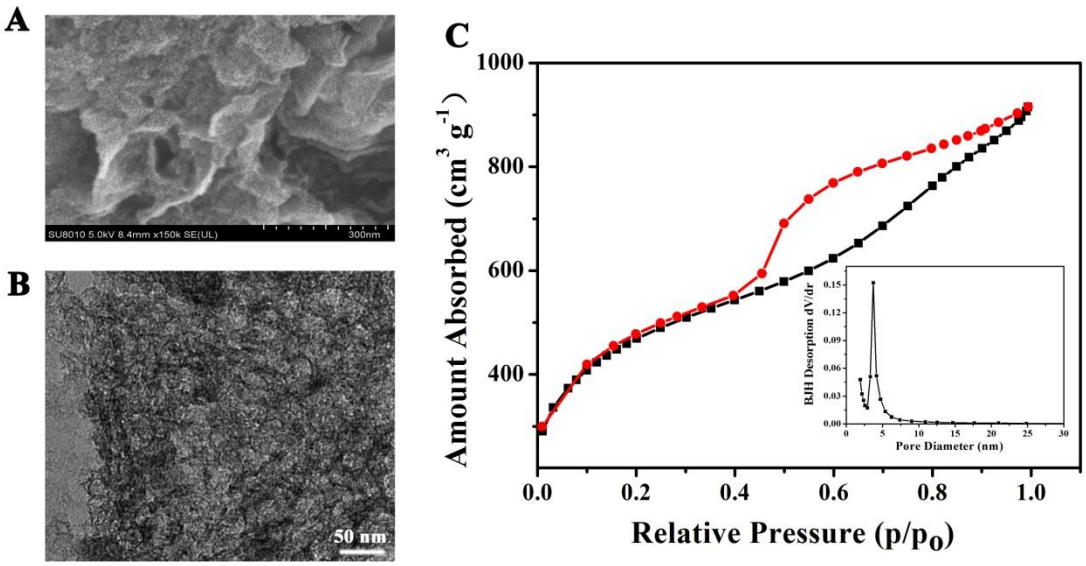

Figure 1. (A) SEM images of 3D-NNPCs. (B) TEM images of 3D-NNPCs. (C) Nitrogen adsorption-desorption isotherms of 3D-NNPCs. Inset: pore size distribution for 3D-NNPCs.

To further study the pore structure of 3D-NNPCs, N_2 adsorption-desorption isothermal analysis was performed, as shown in Figure 1C. It was typically a type IV adsorption-desorption isotherm with a hysteresis loop within a relative pressure range of 0.4-1.0 [30, 31]. Therefore, it can be suggested that 3D-NNPCs have a prolific mesoporous structure. The hierarchical mesopores in 3D-NNPCs are also verified by the wide pore size distribution centred at 3.67 nm (insets in Figure 1C), demonstrating that

the pores were mainly in the region of large micropores and small mesopores. The specific surface area of the 3D-NNPCs is calculated to be 1683.54 $m^2 g^{-1}$ based on the Brunauer-Emmett-Teller (BET) model, while the pore volume is up to 1.09 $cm^3 g^{-1}$ using the BJH model [32]. The high specific surface area and pore volume of 3D-NNPCs at the electrode/electrolyte interface provide a favourable path for electrolyte diffusion and mass transfer, enabling it to be a promising electrode material for electrocatalysis [33].

Figure 2A displays the XRD patterns of the prepared 3D-NNPCs, which exhibit two characteristic diffraction peaks centred at 23.7° and 43.6° that can be assigned to the (002) plane and (101) plane of graphitic carbon [34]. Raman spectroscopy, a characterization technique for carbonaceous materials [35], is recorded for the 3D-NNPCs, as shown in Figure 2B. It exhibits two bands at 1407.98 cm^{-1} and 1440.16 cm^{-1}, corresponding to the D band (originating from the disordered carbon structure and crystal defects [36] and G band (related to the sp^2 hybridized carbon atoms [36]), respectively. The number of defect sites in materials is proportional to the ratio of the relative intensity of the D band and G band (I_D/I_G) [36]. The prepared 3D-NNPCs have an I_D/I_G value of 1.36 suggesting a high density of defective sites on the surface of the material and is higher than that of reported carbon nanotubes [37]. The structural defects on the surface of 3D-NNPCs is favourable for improving the electrocatalysis performance [38].

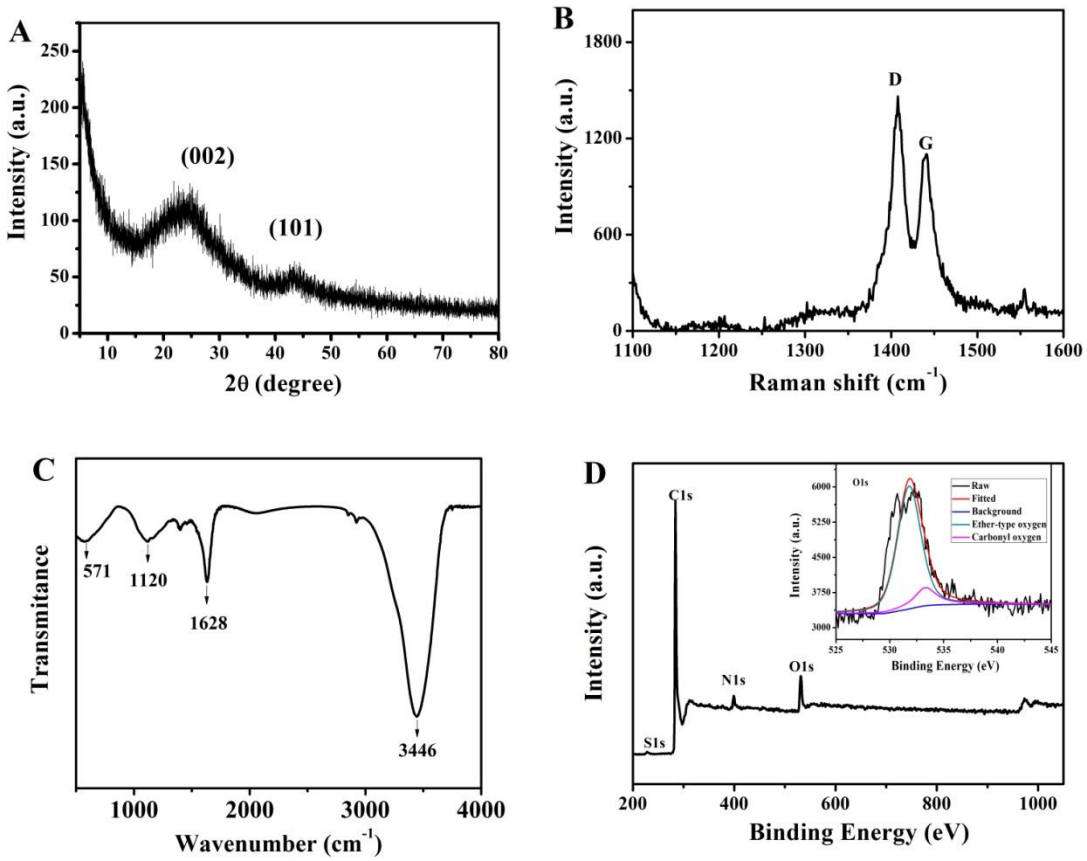

Figure 2. (A) XRD pattern of 3D-NNPCs. (B) Raman spectrum of 3D-NNPCs. (C) FT-IR spectrum of 3D-NNPCs. (D) XPS spectrum of 3D-NNPCs. Inset: high-resolution XPS spectrum of O 1s.

The 3D-NNPCs were further investigated by FT-IR spectroscopy. A band representing an O-H stretching vibration appears at approximately 3446 cm^{-1}, and three bands at 1628, 1120 and 571 cm^{-1} correspond to the characteristic absorption of C=C, C-O and aromatic C-H, respectively (Figure 2C) [39]. XPS analysis is used to further certify the chemical or elemental composition, atomic valence state, and surface energy state distribution of the constituent elements in the as-prepared 3D-NNPCs [40, 41]. In Figure 2D, there are four main peaks at 163.36, 284.19, 399.73, 531.85 eV in the measured spectrum (corresponding to the characteristic peaks of S 2p, C 1s, N 1s and O 1s, respectively) without other obvious peaks from metallic species. The relative atom percentages of S, C, N, and O are 1.15%, 86.16%, 5.4% and 7.13%, respectively. The appearance of N in 3D-NNPC/GCE can facilitate the generation of more defect sites, consequently exposing more active sites and improving the electrocatalytic activity of the materials [42-44]. In addition, we can distinguish two peaks at 532.2 eV and 533.7 eV in the high resolution spectrum of oxygen, which is attributed to carbonyl oxygen of keto and quinine, and noncarbonyl oxygen atoms in anhydrides and esters, respectively [45].

3.2. Electrochemical evaluation

As a comparison, an electrochemical sensing interface based on the bare GCE, MWCNT-modified GCE (MWCNT/GCE) and 3D-NNPC/GCE are first examined by CV in 10 mM $K_3Fe(CN)_6/K_4Fe(CN)_6$ containing 0.1 M KCl at a scan rate of 0.1 V/s (Figure 3A). All the three electrodes exhibit a pair of well-defined redox peaks.

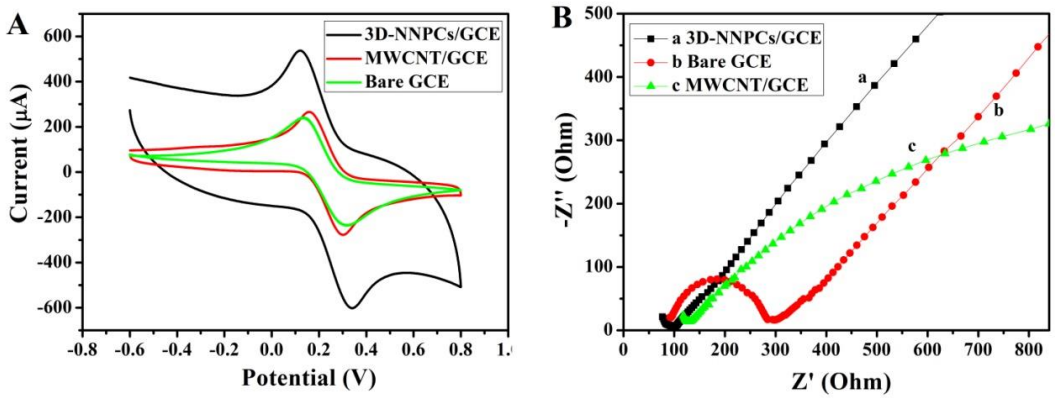

Figure 3. (A) CVs of the bare GCE (green line), MWCNT/GCE (red line) and 3D-NNPC/GCE (black line) in 10 mM $K_3Fe(CN)_6/K_4Fe(CN)_6$ containing 0.1 M KCl at scan rate of 0.1 V/s. (B) EIS of the differently modified electrodes: bare GCE (b), MWCNT/GCE (c) and 3D-NNPC/GCE (a) in 10 mM $K_3Fe(CN)_6$ and $K_4Fe(CN)_6$ containing 0.1 M KCl.

However, in comparison with those of the bare GCE and MWCNT/GCE, the 3D-NNPC/GCE displays the smallest peak-to-peak potential difference (ΔE_p) and highest peak current. For a reversible process monitored by CV, the effective surface area of the working electrode can be estimated according to the Randles-Sevcik [46] equation using a diffusion coefficient of 7.6×10^{-6} cm^2 s^{-1} for $K_3[Fe(CN)_6]$. The electroactive surface area of the 3D-NNPC/GCE can achieve 0.19 cm^2, which is higher than that of

the bare GCE (0.07 cm^2) or the MWCNT/GCE (0.12 cm^2). This is consistent with the result that a larger background current on the 3D-NNPC/GCE was obtained compared to those of the bare GCE or MWCNT/GCE [47]. As indicated above, for electrocatalysis applications, fast mass transfer and high surface areas are desired, and the introduction of hierarchical pore structures is advantageous. The electrochemical behaviour of $K_3Fe(CN)_6/K_4Fe(CN)_6$ on the 3D-NNPC/GCE indicates the potential electrocatalytic performance of this material. Moreover, from the diameter of the semicircle at a high frequency of EIS, the charge transfer resistance (R_{ct}) of different electrodes can be obtained. As shown in Figure 3B, the 3D-NNPC/GCE exhibits the lowest R_{ct} compared to those of the bare GCE and MWCNT/GCE. The above result is attributed to the fact that 3D-NNPCs possess superior conductivity and a large electrochemically active surface area, which provides an outstanding electrochemical response from the electrolyte to the electrode [48].

3.3. Electrocatalytic performance of the 3D-NNPC/GCE for AA detection

Next, using AA as a model, the electrochemical response of the bare GCE, MWCNT/GCE and 3D-NNPC/GCE were studied using CV from -0.40 to 0.60 V in 0.1 M phosphate buffer containing 0.1 M NaCl at pH 7.5. The same concentration of AA solution on the differently modified electrodes exhibits different electrochemical activity. Figure S2 (Supporting Information) shows that with the bare GCE, AA only has a weak irreversible oxidation peak at 0.42 V. With the MWCNT/GCE, the oxidation potential of AA shifts to 0.032 V (vs. Ag/AgCl), and the peak current is greatly enhanced. For the 3D-NNPC/GCE, compared to that of the bare GCE, the peak potential of AA oxidation is negatively shifted by 0.435 V (at -0.015 V vs. Ag/AgCl), and the peak current significantly increases. The high current response and the greatly decreased overpotential indicate that the 3D-NNPC/GCE possesses outstanding electrocatalytic activity towards AA in 0.1 M phosphate buffer containing 0.1 M NaCl (pH 7.5). The reason is that the unique 3D porous structure of the as-prepared material has fast mass transfer, superior conductivity and high surface areas, making the charge transfer much more efficient.

3.3.1. Optimization of AA detection

To quantitatively monitor the concentration of AA, experimental conditions for AA detection were optimized. First, the pH value for the determination is monitored. The influence of pH on the electrochemical behaviour of 3 mM AA is investigated by CV (Figure S3A in Supporting Information). AA oxidation exhibits different peak potentials and peak currents at different pH values. As shown in Figure S3B (Supporting Information), when the pH increases in the pH range of 4.5-8.5, the peak current first increases and then decreases. The maximum peak current for AA oxidation appears at pH 7.5. Therefore, 7.5 is selected as the optimal pH for the detection of AA in the following experiment.

3.3.2. Effect of scan rate

Furthermore, the influence of the scan rate on the response of the electrochemical sensing interface was examined in the presence of 3 mM AA in 0.1 M phosphate buffer containing 0.1 M NaCl

(pH=7.5) (Figure S4A in Supporting Information). The anodic peak current is proportional to the scan rate (Figure S4B in Supporting Information), and the linear equation is I_{pa} (μA) =58.27602 v (V·s^{-1}) +14.81367 (R=0.998). This result indicates that the electrochemical oxidation of AA on the surface of the 3D-NNPC/GCE is an adsorption-controlled process. From the above discussion, AA oxidation is an irreversible process. To obtain the electron transfer rate constant k_s, the logarithm of the scan rate (log$v$) vs. the oxidation peak potential is plotted. As shown in Figure S4C, E_{pa} linearly increases with log$v$, and the linear regression equation is E_{pa}=0.0922log$v$-0.18096 (R=0.998). Based on the Laviron equation [49-51] and from the slope of E_{pa} vs. log$v$, the k_s for the electrochemical oxidation of AA using the 3D-NNPC/GCE is calculated as 0.57 s^{-1}.

3.3.3. Sensitivity of the AA detection

To obtain the sensitivity of the AA detection, DPV was adopted for quantitative analysis of AA (Figure 4A). The peak current increases when the concentration of AA increases. As displayed in Figure 4B, the oxidation peak currents linearly increase as the concentration of AA increases from 1-10000 μM. The linear regression equation is as follows: I_{pa} (μA)= 0.01045C(μM) + 1.5349 (R=0.986). The detection limit is calculated to be 3.76×10^{-7} M (based on 3s_b/S, where s_b is the standard deviation of 20 blank measurements and S is the slope of the analytical curve) with a sensitivity of 0.055 μA·μM^{-1}·cm^{-2}. Based on the high specific surface area, high conductivity and increased number of defective sites on the surface of the 3D-NNPC/GCE, the new sensing interface achieves a low limit of detection and a wide linear range. Consequently, the prepared 3D-NNPCs can be used as a superior material in an electrochemical analysis of AA. A comparison between the results obtained by this work and previously reported electrochemical sensors based on various carbon materials for AA determination is presented in Table 1. The detection limit of our AA sensor is comparable to or lower than most reported AA sensors. Although the sensitivity is not higher, the wide linear range spanning 4 orders of magnitude is very appealing in real applications.

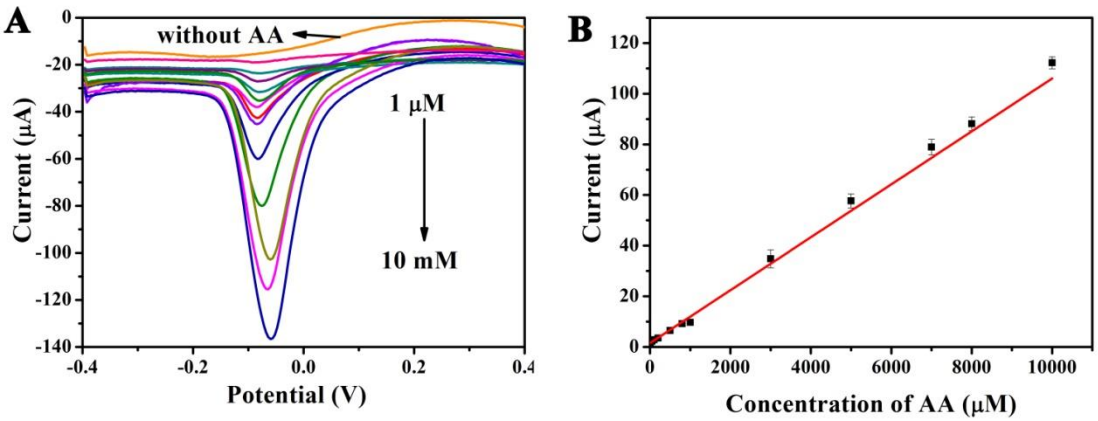

Figure 4. (A) DPV for different concentrations of AA with the 3D-NNPC/GCE in 0.1 M phosphate buffer containing 0.1 M NaCl (pH 7.5) (from top to bottom: 0, 1, 10, 50, 100, 200, 500, 800, 1000, 3000, 5000, 7000, 8000, and 10000 μM). (B) Corresponding calibration curve of peak current versus concentration of AA.

Table 1. Comparison of previously reported electrochemical sensors based on various carbon materials with the electrochemical sensor of this study for AA detection

Electrode	Methods	Linear range (μM)	LOD (μM)	Sensitivity ($\mu A \cdot mM^{-1} \cdot cm^{-2}$)	Ref.
Fe_3C@NGCS[a]/GCE	DPV	54-5491	16.7	-	[52]
MoS_2/f-MWCNTs[b]/ZnO/GCE	Amperometry	10-100	1.01	650	[53]
GCHs-CNPTs[c]/GCE	Amperometry	10-3570	1.09	208.63	[54]
CoPc[d]-MWNTs[e]/GCE	Amperometry	10-2600	1	-	[55]
3D-NNC_sHA_s[f]	Amperometry	10-4410	1	283.17	[56]
N-GMNs[g]/GCE	Amperometry	10-5640	0.51	144.65	[57]
MCNRs[h]/GCE	Amperometry	10-2770	2.3	216.91	[58]
RSNMC[i]/GC	CV	5-6000	3	-	[59]
3D-ICNA[j]/GCE	Amperometry	10-390		140	
		390-1490	3.5	110	[60]
		1490-4490		80	
CNs-HMCNAs[k]/GCE	Amperometry	5-350	0.22	71.34	
		350-2100		49.93	[61]
		2100-7700		24.63	
$ZnCl_2$-CF[l]	DPV	0.05-200	0.02	-	[62]
AC[m]	DPV	30-95	4.96	-	[7]
NG[n]	DPV	5-1300	2.2	-	[63]
MCNF[o]/PGE[p]	DPV	100-10000	50	-	[64]
SWCNH[q]/GCE	DPV	30-400	5	-	[65]
ERGO[r]/GCE	DPV	300-2000	300	-	[66]
H-GO[s]/GCE	DPV	1-100	0.3	-	[67]
HCNTs[t]/GCE	DPV	7.5-180	0.92	-	[68]
3D-NNPCs	DPV	1-10000	0.376	55	This work

[a] N-doped graphitic carbon nanosheets.
[b] flower structured molybdenum disulfide decorated zinc oxide-functionalized multiwall carbon nanotubes.
[c] carbon nanoplatelets derived from ground cherry (Physalis peruviana) husks.
[d] cobalt (II) phthalocyanine.
[e] multi-walled carbon nanotubes.
[f] three-dimensional nitrogen-doped nanostructured carbons with hierarchical architectures.
[g] nitrogen-doped graphene-like mesoporous nanosheets.
[h] mesoporous carbon nanorods.
[I] rice starch based nano/mesoporous carbon.
[j] three-dimensional interconnected carbon nanorod aerogel.
[k] carbon nanorods assembled hierarchical meso-macroporous carbons networks aerogels.
[l] kiwifruit skin.
[m] activated carbon.
[n] nitrogen doped graphene.
[o] mesoporous carbon nanofiber.
[p] pyrolytic graphite electrode.
[q] Single-walled carbon nanohorn.
[r] electrochemically reduced graphene oxide.
[s] hemin functionalized graphene oxide.
[t] helical carbon nanotubes.

3.3.4. Selectivity of the AA detection

As an indispensable small biological molecule, AA is widely included in food [69]. However, all kinds of other small molecules, such as UA, DA and GLU, are rich in food, which often leads to

interference during AA detection. A range of small molecules, such as UA, DA, GLU, GSH and L-Cys, are selected to assess the selectivity of the 3D-NNPC/GCE. The effect of other small molecules (10 μM) on the peak current of 1 μM AA is monitored in 0.1 M phosphate buffer containing 0.1 M NaCl (pH 7.5) using DPV. As shown in Figure S5 (Supporting Information), all the added small molecules have no obvious effect on the current of AA for each of three parallel tests. On the 3D-NNPC/GCE surface, the detection of AA shows excellent selectivity, and other coexisting small molecules cannot produce obvious interference.

3.3.5. Reproducibility and stability

To check the reproducibility and stability of the electrode, several successive measurements were conducted every two days for 20 days using the same electrode with 1 μM of AA. Three modified electrodes are used to obtain parallel experimental results. After 20 days of storage, the three modified electrodes retain an average of 75% of their initial current response (the relative standard deviation RSD <4.1%). Although the storage stability is not very good, the reproducibility between the different electrodes is good. The decrease in storage stability may be related to the adsorption-controlled process.

3.3.6. Real sample analysis

Table 2. Determination of AA in a series of diluted food and beverage samples (n = 3)

Sample used	Added (μM)	Found (μM)	Recovery (%)	RSD (%) (n=3)
Milk	10000	10001.4	100.01	2.18
	100	99.93	99.93	3.30.
	10	9.19	91.9	1.3
Beer	10000	10005.7	100.06	1.45
	100	100.32	100.32	2.33
	10	10.1	101.0	2.19
Homemade kiwi juice	10000	9949	99.49	3.38
	100	100.89	100.89	1.91
	10	0.956	95.6	4.11
Homemade tomato juice	10000	9797	97.97	3.95
	100	97.89	97.89	2.34
	10	0.98	98.00	3.50
Honey	10000	9780	97.80	2.53
	100	95.69	95.69	3.67
	10	10.5	105.0	3.27

In addition, to accurately and effectively evaluate the feasibility of the electrochemical sensor in practical applications, the electrochemical determination of AA in practical food samples is investigated. AA (10 μM, 100 μM and 10000 μM) is spiked in diluted food and drinks such as milk, beer, homemade kiwi juice, homemade tomato juice and honey. The recovery rate is monitored according to the obtained

value of the peak current. As shown in Table 2, the recoveries ranged from 91.9%~105.0% (n=3), which indicates the potential feasibility of the electrochemical sensor for the detection of AA in food.

3.4. Electrochemical response to other biomolecules

Furthermore, some important biomolecules, such as DA, UA, GLU, GSH and Tyr, were also tested using the new sensing system. As shown in Figure 5, at 3D-NNPC/GCE, the abovementioned biomolecules all produce very strong electrochemical signals. Compared with that of the bare GCE, a greatly increased current is obtained for UA on the 3D-NNPC/GCE (Figure 5A). For DA (Figure 5B), GSH (Figure 5C), Tyr (Figure 5D) and GLU (Figure 5E), both a large increase in the anodic current and a decrease in the oxidation peak potential are achieved. The 3D-NNPC/GCE has a faster electron transfer rate than the bare GCE, which may provide 3D-NNPCs with wide application potential in electrocatalysis.

Furthermore, for potentially wide application of the electrochemical sensing interface based on the 3D-NNPC/GCE, the electrocatalytic activity of the 3D-NNPC/GCE is exploited for the simultaneous detection of three biomolecules using DPV by keeping the concentrations of the two analytes constant and varying the concentration of the third analyte.

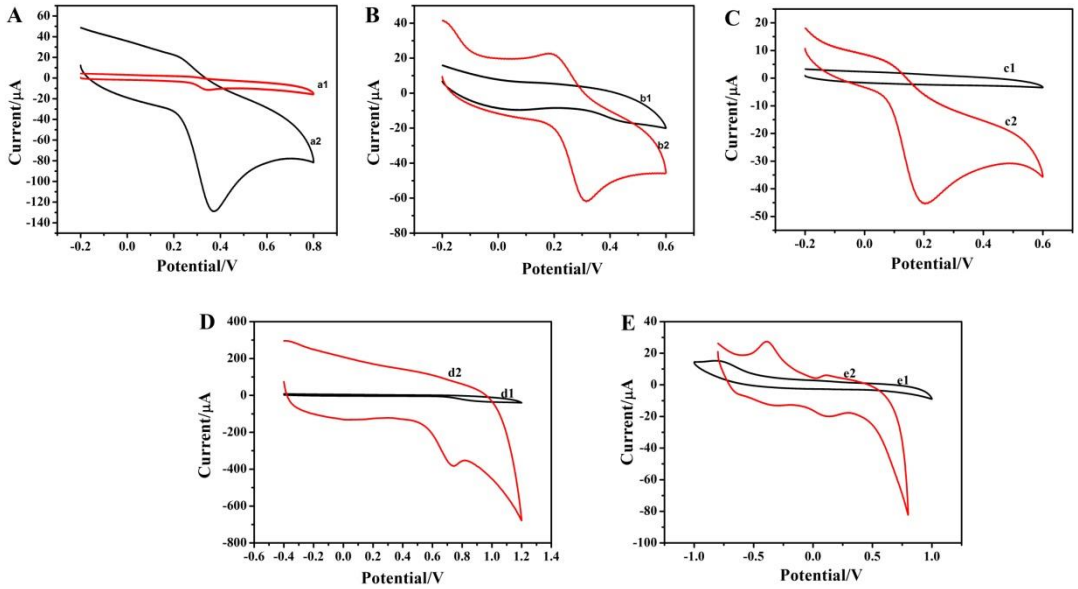

Figure 5. (A) CV curves for 5 mM UA with the bare GCE (a1) and 3D-NNPC/GCE (a2). (B) CV curves for 5 mM DA with the bare GCE (b1) and 3D-NNPC/GCE (b2). (C) CV curves for 5 mM GSH with the GCE (c1) and 3D-NNPC/GCE (c2). (D) CV curves for 5 mM Tyr with the GCE (d1) and 3D-NNPC/GCE (d2). (E) CV curves for 5 mM GLU with the GCE (e1) and 3D-NNPC/GCE (e2). Test conditions: scan rate, 0.1 $V \cdot s^{-1}$; electrolyte, 0.1 M phosphate buffer containing 0.1 M NaCl (pH 7.5).

As shown in Figure S6A (Supporting Information), in the presence of two other molecules, AA and DA, the oxidation peak current of UA increases gradually with increasing concentration of UA,

showing good electrocatalytic activity on the 3D-NNPC/GCE. The linear range for UA is from 1 mM to 50 mM, and the linear regression equation is I_{pa} (μA)=0.00343C(μM) + 18.89431 (R=0.987) (Figure S6B in Supporting Information). In addition, the simultaneous detection of multiple substances, including AA, DA and UA, is attempted, and the results are not very good due to the mutual interference of the two close peaks at low concentrations.

4. CONCLUSIONS

In conclusion, a simple method for preparing 3D-NNPCs with high surface areas and high densities of defective sites based on an abundant and edible alga has been proposed. The prepared 3D-NNPCs were characterized by various methods. The incorporation of multiple types of pores makes 3D-NNPCs beneficial for the electrocatalysis of small molecules. AA was first used as a model for electrochemical sensing using this material. An extremely wide linear range and good selectivity were obtained. The potential feasibility of the electrochemical sensor for detecting AA in food was also demonstrated. Finally, a potentially wide application of the electrochemical sensing interface based on the 3D-NNPC/GCE was demonstrated; the sensor had good electrocatalytic performance for other biomolecules with a large increase in oxidation peak current and a large decrease in overpotential.

DECLARATION OF COMPETING INTEREST

The authors declare no competing financial interest.

ACKNOWLEDGEMENTS

This work was supported by the Key Research and Development Program of Shandong Province, China (2019GSF111047) and the Natural Science Foundation of Shandong Province, China (ZR2019MB019).

SUPPORTING INFORMATION

Figure S1. Fresh *Ulva lactuca* L.

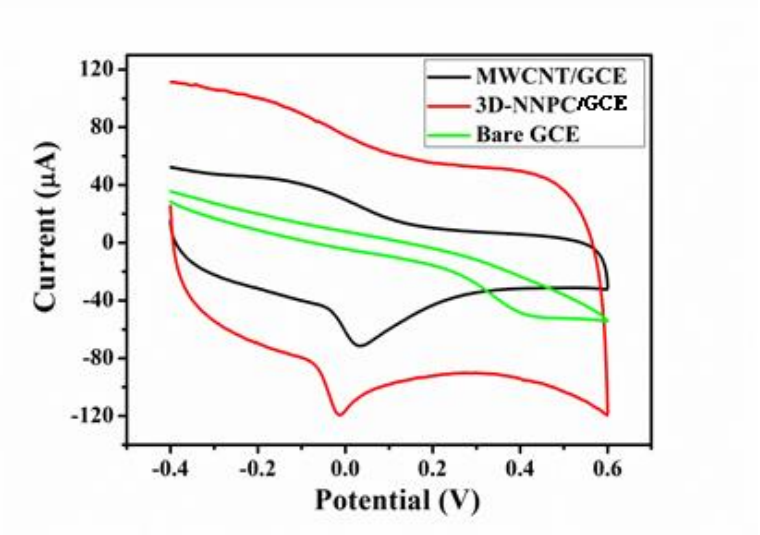

Figure S2. CV curves of 3 mM AA with the differently modified electrodes in 0.1 M phosphate buffer containing 0.1 M NaCl at pH 7.5.

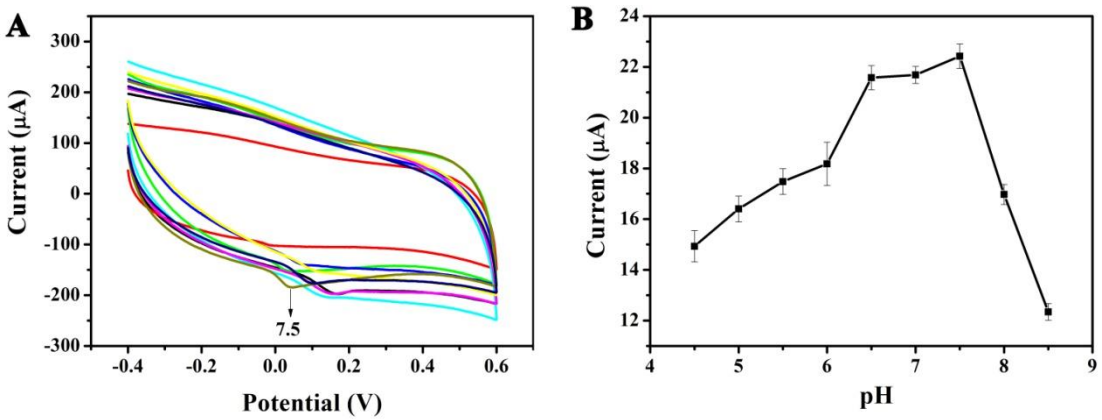

Figure S3. (A) CV curves of the modified 3D-NNPC electrode at different pH values containing 3 mM AA at a scan rate of 0.1 V/s in 0.1M phosphate buffer containing 0.1 M NaCl (pH 4.5-8.5). (B) The curve of the peak current of AA vs. pH.

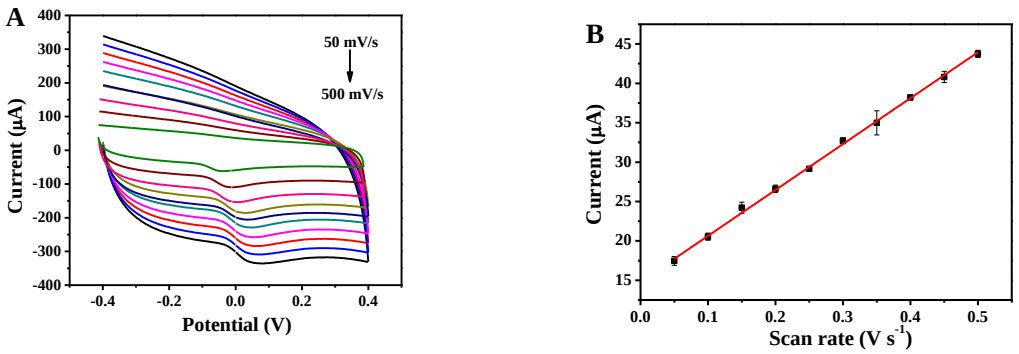

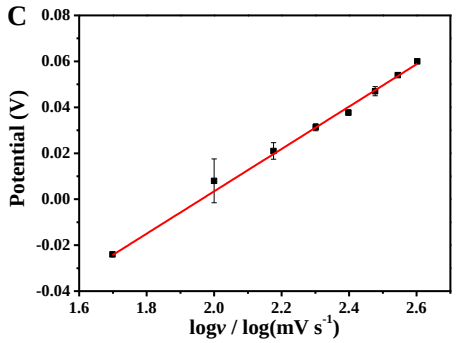

Figure S4. (A) CV curves of 3 mM AA at different scan rates (50, 100, 150, 200, 250, 300, 350, 400, 450 and 500 mv·s^{-1}). (B) The linear relation of the anodic peak currents against the scan rates in the range of 50 to 500 mV·s^{-1}. (C) Relationship of the anodic peak potential vs. the scan rates.

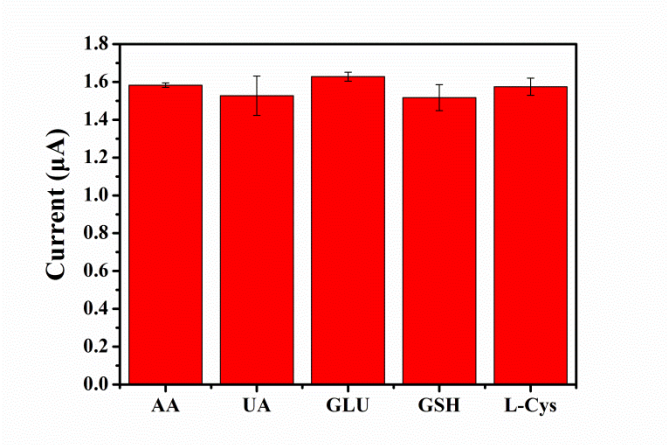

Figure S5. The effect of 10 μM UA, GLU, GSH and L- Cys on the peak current of 1 μM AA. Error bars show the deviation of measurements obtained via three independent surveys. All experiments were conducted in 0.1 M phosphate buffer containing 0.1 M NaCl (pH 7.5).

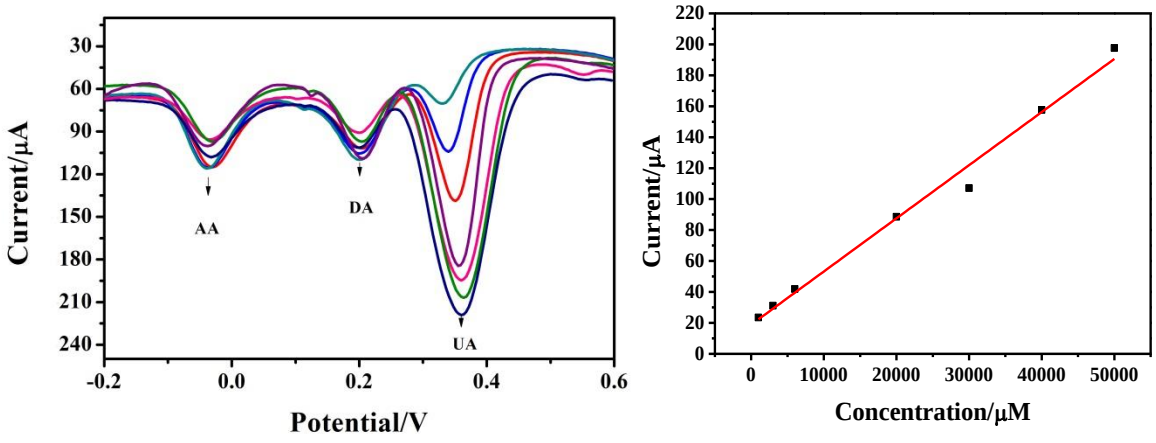

Figure S6. DPV response with the 3D-NNPC/GCE in 0.1 M PBS (pH=7.4) with a UA range from 1000 μM to 50000 μM containing 5 μM AA and DA

References

1. D.Q. Kong, S. Bi, Z.H. Wang, J.F. Xia, F.F. Zhang, *Anal. Chem*., 88 (2016) 10667.
2. M. Zhou, Y. Zhai, S. Dong, *Anal. Chem*., 81 (2009) 5603.
3. P. Ramnani, N.M. Saucedo, A. Mulchandani, *Chemosphere,* 143 (2016) 85.
4. Z.Y. Wang, Z.H. Dai, *Nanoscale*, 7 (2015) 6420.
5. M.M. Barsan, M.E. Ghica, C.M.A. Brett, *Anal. Chim*., Acta 881 (2015) 1.
6. J. Wang, *Electroanalysis*, 17 (2005) 7.
7. V. Veeramani, R. Madhu, S.M. Chen, B.S. Lou, J. Palanisamy, V.S. Vasantha, *Sci. Rep*., 5 (2015) 10141.
8. M. Zhou, L. Shang, B. Li, L. Huang, S. Dong, *Biosens. Bioelectron*., 24 (2008) 442.
9. W. Zhang, Z.Y. Wu, H.L. Jiang, S.H. Yu, *J. Am. Chem. Soc*., 136 (2014) 14385.
10. A. Mahmood, W.H. Guo, H. Tabassum, R.Q. Zou, *Adv. Energy Mater*., 6 (2016) 1600423.
11. P.Q. Liao, J.Q. Shen, J.P. Zhang, *Coordin. Chem. Rev*., 373 (2018) 22.
12. N.P. Wickramaratne, J.T. Xu, M. Wang, L. Zhu, L.M. Dai, M. Jaroniec, *Chem. Mater*., 26 (2014) 2820.
13. F. Xu, Z.W. Tang, S.Q. Huang, L.Y. Chen, Y.R. Liang, W.C. Mai, H. Zhong, R.W. Fu, D.C. Wu, *Nat. Commun*., 6 (2015) 7221.
14. L. Wan, J.L. Wang, Y.H. Sun, C. Feng, K.X. Li, Rsc Adv., 5 (2015) 5331.
15. R. Vinodh, A. Abidov, M.M. Peng, C.M. Babu, M. Palanichamy, W.S. Cha, H.T. Jang, *J. Ind. Eng. Chem*., 32 (2015) 273.
16. A. Ganesan, R. Mukherjee, J. Raj, M.M. Shaijumon, *J. Porous Mater*., 21 (2014) 839.
17. W.J. Qian, F.X. Sun, Y.H. Xu, L.H. Qiu, C.H. Liu, S.D. Wang, F. Yan, *Energy Environ. Sci*., 7 (2014) 379.
18. L. Zhu, Y. Wang, Y.X. Wang, L.J. You, X.Q. Shen, S.J. Li, *Microporous Mesoporous Mater*., 241 (2017) 285.
19. B. Henriques, A. Teixeira, P. Figueira, A.T. Reis, J. Almeida, C. Vale, E. Pereira, *Sci. Total Environ.*, 652 (2019) 880.
20. D.E. Onwuegbuchunam, T.E. Ebe, L.I. Okoroji, A.E. Essien, *J. Mar. Sci. Eng*., 5 (2017) 39.
21. J.S. Chang, T. Chienchang, *Bull. Fish. Res. Agency*, (2010) 11.
22. X. Song, L. Huang, J. Zhang, H. Huang, T. Li, Q. Su, *Mar. Pollut. Bull.*, 58 (2009) 1310.
23. S.J. Li, K.H. Han, J.X. Li, M. Li, C.M. Lu, *Microporous Mesoporous Mater.*, 243 (2017) 291.
24. M. Zhou, J. Catanach, J. Gomez, S. Richins, S.G. Deng, *Acs Appl. Mater. Interfaces*, 9 (2017) 4362.
25. M. Ren, T. Zhang, Y. Wang, Z. Jia, J. Cai, *J. Mater. Sci*., 54 (2019) 1606.
26. W.H. Yu, H.L. Wang, S. Liu, N. Mao, X. Liu, J. Shi, W. Liu, S.G. Chen, X. Wang, *J. Mater. Chem. A*, 4 (2016) 5973.
27. H.K.D. Nguyen, H.Q. Tran, N.L.T. Nguyen, N.T. Dinh, *J. Porous Mater*., 25 (2018) 1567.
28. Y.B. Cui, H.X. He, J.D. Atkinson, *Acs Sustainable Chem. Eng*., 7 (2019) 1279.
29. L. Lu, X. Jiao, J. Fan, W. Lei, Y. Ouyang, X. Xia, Z. Xue, Q. Hao, Electrochim. Acta, 295 (2019) 461.
30. X. Yang, W. Zou, Y. Su, Y. Zhu, H. Jiang, J. Shen, C. Li, *J. Power Sources*, 266 (2014) 36.
31. R. Madhu, K.V. Sankar, S.M. Chen, R.K. Selvan, *Rsc Adv*., 4 (2013) 1225.
32. F.P. Hu, Z. Wang, Y. Li, C. Li, X. Zhang, P.K. Shen, *J. Power Sources*, 177 (2008) 61.
33. T. Mesarič, L. Baweja, B. Drašler, D. Drobne, D. Makovec, P. Dušak, A. Dhawan, K. Sepčić, Carbon, 62 (2013) 222.
34. Y. Xia, Z. Yang, R. Mokaya, Chem. Mater., 18 (2006) 140.
35. D. Graf, F. Molitor, K. Ensslin, C. Stampfer, A. Jungen, C. Hierold, L. Wirtz, *Nano Lett*., 7 (2007) 238.
36. A.C. Ferrari, J. Robertson, *Phys. Rev. B*, 61 (2000) 14095.

37. M. Zhou, L. Shang, B. Li, L. Huang, S. Dong, *Electrochem. Commun*., 10 (2008) 859.
38. B.Y. Xia, Y. Yan, N. Li, H.B. Wu, X.W. Lou, X. Wang, *Nat. Energy*, 1 (2016) 15006.
39. J.H. Zhou, Z.J. Sui, J. Zhu, P. Li, D. Chen, Y.C. Dai, W.K. Yuan, Carbon, 45 (2007) 785.
40. D. Zhu, H. Ma, H. Pang, L. Tan, J. Jiao, T. Chen, Electrochim. Acta, 266 (2018) 54.
41. Y. Luo, F.-Y. Kong, C. Li, J.-J. Shi, W.-X. Lv, W. Wang, *Sens. Actuators, B*, 234 (2016) 625.
42. Y. Wang, Y.Y. Shao, D.W. Matson, J.H. Li, Y.H. Lin, *Acs Nano*, 4 (2010) 1790.
43. X.A. Xu, S.J. Jiang, Z. Hu, S.Q. Liu, *Acs Nano*, 4 (2010) 4292.
44. Y.F. Tang, B.L. Allen, D.R. Kauffman, A. Star, *J. Am. Chem. Soc*., 131 (2009) 13200.
45. J. Li, K. Liu, X. Gao, B. Yao, K.F. Huo, Y.L. Cheng, X.F. Cheng, D.C. Chen, B. Wang, W.M. Sun, D. Ding, M.L. Liu, L. Huang, *Acs Appl. Mater. Interfaces*, 7 (2015) 24622.
46. S. Hrapovic, Y. Liu, K.B.M. And, J.H.T. Luong, *Anal. Chem*., 76 (2004) 1083.
47. L. Fu, K. Xie, Y. Zheng, L. Zhang, W. Su, *Electronics*, 7 (2018) 15.
48. M. Jin, X. Zhang, Q. Zhen, Y. He, X. Chen, W. Lyu, R. Han, M. Ding, *Biosens. Bioelectron*., 98 (2017) 392.
49. J. Li, Z. Xu, M. Liu, P. Deng, S. Tang, J. Jiang, H. Feng, D. Qian, L. He, *Biosens. Bioelectron*., 90 (2017) 210.
50. E. Laviron, *J. Electroanal. Chem. Interfacial Electrochem.,* 52 (1974) 355.
51. E. Laviron, *J. Electroanal. Chem. Interfacial Electrochem*., 101 (1979) 19.
52. Y. Chen, X.F. Zhang, A.J. Wang, Q.L. Zhang, H. Huang, J.J. Feng, *Microchim. Acta,* 186 (2019) 660.
53. N. Murugan, T.H.V. Kumar, N.R. Devi, A.K. Sundramoorthy, *New J. Chem*., 43 (2019) 15105.
54. X. Li, Y. Wang, J. Liu, M. Sun, X. Bo, H.-L. Wang, M. Zhou, *Electrochem. Commun*., 82 (2017) 139.
55. X. Zuo, H. Zhang, N. Li, *Sens. Actuators B: chem.,* 161 (2012) 1074.
56. Y.S. Hei, X.Q. Li, X. Zhou, J.J. Liu, M. Hassan, S.Y. Zhang, Y. Yang, X.J. Bo, H.L. Wang, M. Zhou, *Anal. Chim. Acta*, 1029 (2018) 15.
57. T.Z. Sha, J.J. Liu, M.M. Sun, L. Li, J. Bai, Z.Q. Hu, M. Zhou, *Talanta*, 200 (2019) 300.
58. X.X. Li, J.J. Liu, M.M. Sun, T.Z. Sha, X.J. Bo, M. Zhou, *Microchim. Acta*, 185 (2018) 474.
59. M.A. Wahab, F. Darain, N. Islam, D.J. Young, *Molecules*, 23 (2018) 234.
60. C.X. Xu, Y.S. Hei, J.J. Liu, M.M. Sun, T.Z. Sha, N. Wang, M. Hassan, X.J. Bo, M. Zhou, *Microchim. Acta*, 185 (2018) 482.
61. N. Wang, Y.S. Hei, J.J. Liu, M.M. Sun, T.Z. Sha, M. Hassan, X.J. Bo, Y.N, Guo, M. Zhou, *Anal.Chim. Acta*, 1047 (2019) 36.
62. W.J. Zhang, L. Liu, Y.G. Li, D.Y. Wang, H. Ma, H.L. Ren, Y.L. Shi, Y.J. Han, B.C. Ye, *Biosens. Bioelectron.,* 121 (2018) 96.
63. Z.H. Sheng, X.Q. Zheng, J.Y. Xu, W.J. Bao, F.B. Wang, X.H. Xia, *Biosens. Bioelectron.*, 34 (2012) 125.
64. Y. Yue, G.Z. Hu, M.B. Zheng, Y. Guo, J.M. Cao, S.J. Shao, *Carbon*, 50 (2012) 107.
65. S.Y. Zhu, H.J. Li, W.X. Niu, G.B. Xu, *Biosens. Bioelectron.*, 25 (2009) 940.
66. L. Yang, D. Liu, J.S. Huang, T.Y. You, *Sens. Actuators B: chem.*, 193 (2014) 166.
67. H.L. Zou, B.L. Li, H.Q. Luo, N.B. Li, *Sens. Actuators B: chem.,* 207 (2015) 535.
68. R.J. Cui, X.Y. Wang, G.H. Zhang, C. Wang, *Sens. Actuators B: chem.,* 161 (2012) 1139.
69. J.S. Lee, Y. Chang, E.S. Lee, H.G. Song, P.S. Chang, J. Han, *J. Food Sci*., 83 (2018) 682.